

Roughening and facet formation in the presence of subharmonic potentials

J. A. Jaszczak and W. F. Saam

Department of Physics, The Ohio State University, Columbus, Ohio 43210

(Received 21 September 1987; revised manuscript received 22 December 1987)

Roughening transitions are explored as a function of the strength V_2 of a subharmonic potential, which can be varied with the chemical potential difference in a two-component crystal like galena (PbS) or one of its analogs (e.g., SnTe). The dependence of both the facet size and the step energy on V_2 are given, for small V_2 , explicitly in terms of the surface stiffness at $V_2=0$. A close connection of the model to the F model is exploited to obtain hitherto inaccessible features of the F model phase diagram in direct and staggered fields.

I. INTRODUCTION

Roughening and facet formation have been explored in some detail, both experimentally¹⁻⁴ and theoretically,⁵⁻¹⁰ during the past several years. In particular, the prediction⁶ of a universal curvature (or surface stiffness) at the roughening temperature has been verified to good accuracy.² The relevant theory can be conveniently discussed in terms of sine-Gordon picture,^{1,11-13} with a Hamiltonian

$$H = \int d\mathbf{r} \left[\frac{\sigma}{2} |\nabla z(\mathbf{r})|^2 - \frac{V_1}{a^2} \cos \frac{2\pi z(\mathbf{r})}{b} \right], \quad (1)$$

in which $\mathbf{r}=(x,y)$, $z(\mathbf{r})$ is the local fluid-solid interface position variable, σ is a microscopic surface stiffness, a is an in-plane lattice constant, and b is an out-of-plane lattice constant. V_1 is the strength of the periodic potential which expresses the preference of the system to place the interface at integral heights in units of b .

In this work, we shall be particularly interested in a generalization of H to a situation where an additional, subharmonic, periodic potential is present so that H becomes

$$H = \int d\mathbf{r} \left[\frac{\sigma}{2} |\nabla z(\mathbf{r})|^2 - \frac{V_1}{a^2} \cos \frac{2\pi z(\mathbf{r})}{b} - \frac{V_2}{a^2} \cos \frac{\pi z(\mathbf{r})}{b} \right]. \quad (2)$$

Such a Hamiltonian may be thought of as describing a two-component system, composed of atoms of types A and B , where the natural crystal structure places alternating layers of A and B perpendicular to the z axis. As a concrete example, we suggest one of the IV-VI semiconductors, such as galena (PbS) or SnTe when the z axis is along the [111] direction. The SnTe crystal in this direction is built from alternating triangular layers of Sn and Te. While the IV-VI compounds are isostructural with NaCl,^{14,15} the bonding is much less ionic.¹⁶ The covalent nature of the bonding tends to compensate for the difference in electronegativities between Sn and Te, resulting in a more neutral bond.¹⁷ According to Ref. 16,

“it is possible to use the terms of the theory of close packing of atoms in describing and interpreting these structures.” Also unlike NaCl, natural crystals of galena (PbS) and altaite (PbTe) commonly exhibit {111} facets.¹⁸ The similarity in the electronegativities, atomic radii, and the atomic electron configurations of Sn and Te atoms suggest that along [111] in SnTe the alternating Sn and Te layers are energetically equivalent.¹⁹ Positive (negative) V_2 may then be identified with a preference for the first crystalline layer to consist of Sn (Te). This preference will be realized in a situation where the fluid in equilibrium with the crystal contains an excess of Sn. More formally, variation of V_2 is affected by variation of the Sn-Te chemical potential difference.

Nienhuis, Hilhorst, and Blöte⁹ (NHB) have noted the existence of roughening transitions as a function of subharmonic potentials in solid-on-solid (SOS) models in general. Within a specific model (the triangular Ising SOS model) full details were worked out. However, this model suffers the drawback that the temperature could not be explicitly varied. In this work, we discuss in some detail the roughening transition of the model specified by Eq. (2) as a function of T and V_2 , making predictions directly accessible to experiment. In addition, we discuss the relation of the model of Eq. (2) to the F model,²⁰ noting that V_2 corresponds to a staggered electric field in that model, and obtaining hitherto unnoticed results for the phase diagram of the F model.

In Sec. II roughening transitions as functions of V_2 and T are discussed, particular attention being paid to the V_2 dependence of facet size. Section III makes contact with the F model, and Sec. IV contains further discussion. Some details relevant to Sec. II are relegated to the Appendix.

II. ROUGHENING TRANSITIONS

When $V_2=0$, the model of Eq. (2) is well understood.¹⁰⁻¹³ In this case, the (renormalized) macroscopic surface stiffness $\bar{\sigma}$ obeys^{6,21}

$$\frac{\bar{\sigma}(T_{R_1})}{k_B T_{R_1}} = \frac{\pi}{2b^2} \quad (3)$$

at the roughening temperature T_{R_1} in the presence of the period-one potential V_1 . For $V_1=0$ and $V_2 \neq 0$, one has similarly,

$$\frac{\bar{\sigma}(T_{R_2})}{k_B T_{R_2}} = \frac{\pi}{2(2b)^2} = \frac{\pi}{8b^2}. \quad (4)$$

For weak potentials, $\bar{\sigma}(T_{R_1})$ and $\bar{\sigma}(T_{R_2})$ differ little from σ , so that the approximate relation $T_{R_2} \approx 4T_{R_1}$ holds. (More generally, $T_{R_p} \sim p^2$, where p is the period, for weak potentials.) For given $V_1 \neq 0$, turning on V_2 immediately raises the system's true roughening temperature to T_{R_2} as V_2 will be relevant for $T < T_{R_2}$. Facets thus appear in the interval $T_{R_1} < T < T_{R_2}$, and these facets will vanish as $V_2 \rightarrow 0$ in a roughening transition different from the conventional one.

The description of the facet size R_f as $V_2 \rightarrow 0$ is straightforward. One finds, in fact,

$$R_f \sim V_2^x, \quad T_{R_1} < T < T_{R_2}^0, \quad (5)$$

where

$$x = \frac{1}{2} \left[1 - \frac{\bar{\sigma}^0(T_{R_1})T}{4\bar{\sigma}^0(T)T_{R_1}} \right]^{-1} = \frac{1}{2} \left[1 - \frac{\pi k_B T}{8b^2 \bar{\sigma}^0(T)} \right]^{-1} \quad (6)$$

and $\bar{\sigma}^0(T)$ is the macroscopic surface stiffness at $V_2=0$. In Eq. (5), $T_{R_2}^0$ is the limit of T_{R_2} for small V_2 . It is important to note that the exponent x is determined entirely by the *experimentally accessible* quantities $\bar{\sigma}^0$ and b . Furthermore, x is a temperature-dependent critical exponent varying from $\frac{2}{3}$ at T_{R_1} to ∞ at $T_{R_2}^0$.

The derivation of Eq. (6) is simple, amounting largely to a rewriting of arguments of NHB. The critical index y_2 of the field V_2 at the fixed line ($T > T_{R_1}$) of the model with $V_2=0$, $V_1 \neq 0$ is²²

$$y_2 = 2 - \frac{\pi k_B T}{4b^2 \bar{\sigma}^0(T)}. \quad (7)$$

At the fixed line, V_1 has renormalized to zero, its effects being incorporated in the macroscopic stiffness $\bar{\sigma}^0(T)$. For $y_2 > 0$, V_2 is relevant, and $T_{R_2}^0$ is determined by $y_2(T_{R_2}^0) = 0$. To connect this result to the facet size, we merely note that in renormalization at length scale l , $V_2(l)$ (the value to which V_2 renormalizes) obeys

$$\frac{d \ln V_2}{d \ln l} = y_2, \quad (8)$$

the integration of which gives the dependence of the correlation length ξ on the initial value of V_2 as

$$\xi \sim (V_2)^{-1/y_2}. \quad (9)$$

The facet size R_f goes inversely as the correlated length,⁶ so that the result Eq. (6) follows with $x = 1/y_2$. The clear connection of x with the stiffness $\bar{\sigma}^0(T)$ was not noted by NHB. Note also that the step energy is proportional to

ξ^{-1} .⁶ It is of some interest to look more closely at the interplay between the potentials V_1 and V_2 as renormalization proceeds. This is done in the Appendix.

III. CONNECTION TO THE F MODEL

The F model²⁰ has a well-known connection to roughening and facet formation via its equivalence to the body-centered solid-on-solid (BCSOS) (Refs. 6 and 23) and face-centered solid-on-solid (FCSOS) (Ref. 7) models. This connection has been made for zero staggered field E_s but for nonzero direct field E , the direct field corresponding to coordinates used in drawing the crystal shape.⁶⁻⁹ Here we point out that a staggered field in the F model plays the role of V_2 in the model of Eq. (2). We use the results of Sec. I to derive new results for the F -model phase diagrams for $E_s \neq 0$. The effect of V_1 is, of course, imposed by the lattice.

For $E=0$, $E_s=0$ the F model has two equivalent ground states, A and B , corresponding in the BCSOS model to the $T=0$ (100) crystal surface being formed by atoms at cube corners in one case (A), or at cube centers (B) (half a cubic lattice constant a down). A sloped surface will involve a sequence of steps connecting these states in an alternating fashion ($ABAB\dots$). A staggered

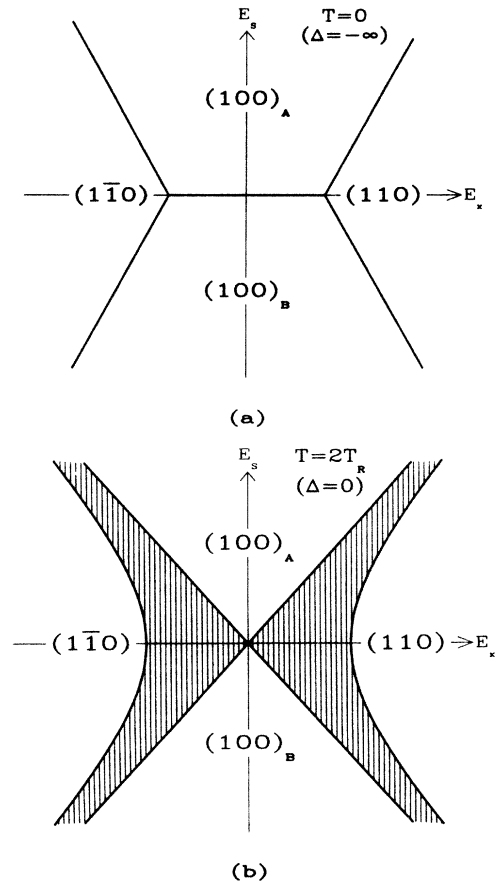


FIG. 1. Phase diagrams (sketched) in E_s - E_x space for the BCSOS model for (a) $T=0$ and (b) $T=2T_R$ ($\Delta=0$). Facets are labeled, and the regions between facets in (b) are rough.

field makes one of these ground states, say A , energetically favored over the other. Thus the A states, separated by $2 \times a/2$ —twice the natural periodicity, are favored. This is precisely the effect of V_2 in the model of Eq. (2).

The phase diagram of the F model for $E_s \neq 0$ and $E_x \neq 0$ is ill understood. It is easy to construct at $T=0$; see Fig. 1(a), where we set $E_y=0$, retaining E_x . \mathbf{E} is rotated by 45° from the underlying F -model lattice. The phases are separated by heavy lines and are labeled by the bcc facet to which they correspond. The width of the $(100)_A$ and $(100)_B$ facets is the horizontal width of the respective unshaded regions, increasing linearly with $|E_s|$. The phase diagram can also be constructed at a special temperature $T > T_{R1}$ known as the $\Delta=0$ point.^{20,24} From Baxter's²⁴ results, we easily arrive at the sketch of Fig. 1(b). The salient feature for our purposes is that the phase boundaries near the origin are straight, showing that the facet size near $E_s=0$ varies linearly with E_s . This is the case where the exponent x of Eq. (6) is unity, corresponding to $\tilde{T}_R=8$, and

$$\tilde{T}_R = \frac{2\pi k_B T}{b^2 \bar{\sigma}^0(T)}. \quad (10)$$

(NHB use the notation T_R for our \tilde{T}_R .) From the fact that the surface stiffness is the second derivative of the free energy with respect to slope, one readily finds the connection

$$\tilde{T}_R = \frac{4\pi}{\pi - \mu} \quad (11)$$

between \tilde{T}_R and the conventional parameter μ ²⁰ of the F model.

The shaded regions of Fig. 1(b) correspond to rough surfaces, and one readily shows from Baxter's solution²⁴ that the phase transition lines are of the Pokrovsky-Talapov type, indicating that the rough surfaces join the facets with exponent $\frac{3}{2}$, as usual.⁵⁻⁹

Next, consider the phase diagram at the F -model roughening temperature $T_R (=T_{R1}$ in the context of this paper) corresponding to $\Delta=-1$; $\tilde{T}_R=4$.²⁰ The (100) facet size is zero at $E_s=0$ and increases as $E_s^{2/3}$ ($x=\frac{2}{3}$) near $E_s=0$. We thus conjecture the phase diagram of Fig. 2(a). The (110) and the (100) facets will have rough regions separating them at any $T > 0$ because of the high degeneracy²⁵ along their common boundary at $T=0$. We conjecture that, as for $\Delta=0$, the phase boundaries are of the Pokrovsky-Talapov type.

We expect a smooth crossover from Fig. 2(a) to Fig. 1(b) as T increases. With further increase in T , the facet size exponent x increases until it reaches 2 at $T=\infty$ ($\Delta=\frac{1}{2}$, $\tilde{T}_R=12$ in the F model²⁰). The phase diagram at $T=\infty$ is sketched in Fig. 2(b). The case $T=T_{R2}$ is not accessible in the F model, as this corresponds to $\tilde{T}_R=16$.

For completeness, we give in Fig. 2(c) our conjectured phase diagram for $0 < T < T_R$ ($-\infty < \Delta < -1$). As mentioned above, there must be rough regions separating facets, and the facet size [the line LR in Fig. 2(c)] at $E_s=0$ is nonzero. The (100) phase boundaries probably intersect L and R linearly, there being no nearby

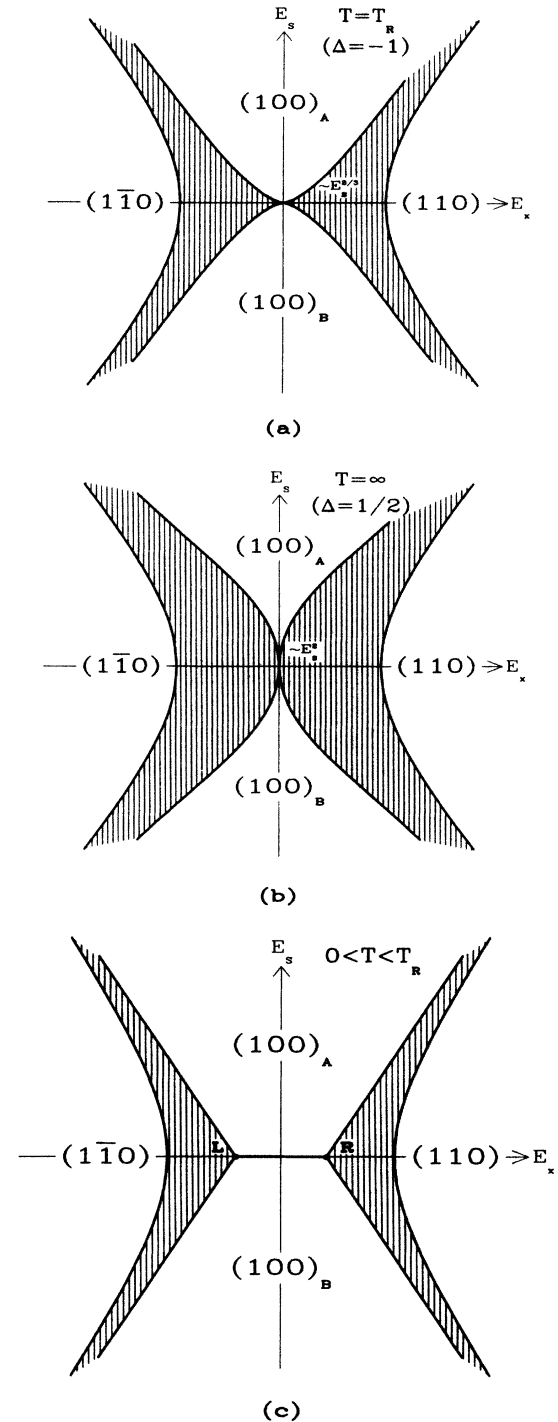


FIG. 2. Conjectured phase diagrams (sketched) in $E_s - E_x$ space for the BCSOS model for (a) $T=T_R$, (b) $T=\infty$, and (c) $0 < T < T_R$.

roughening transition to dictate scaling, in contrast to the $T > T_R$ case.

IV. DISCUSSION

The physics of a model for roughening at a crystal fluid interface has been explored, primarily as regards the effect of a small subharmonic potential. In the tempera-

ture range $T_{R_1} < T < T_{R_2}^0$, roughening occurs with facet sizes vanishing as V_2^x , where the continuously varying exponent x is given as a function of T by Eq. (6). The transition is *not* of the more usual Kosterlitz-Thouless type,^{6,13} and in contrast to that case, the curvature is *not* a universal quantity at the transition. As noted in the Introduction, {111} interfaces of crystals of the SnTe type are good candidates for a test of the results of Eqs. (5) and (6).

This work has also pointed out a close connection between the model of Eq. (2) and the F model (more generally, the antiferroelectric 6-vertex model) in the presence of both direct and staggered electric fields. Certain features of the F -model phase diagram were derived, and it was noted that the $\Delta=0$ solution of Baxter corresponds to the special case $x=1$.

ACKNOWLEDGMENTS

One of us (W.F.S.) wishes to thank H. J. Hilhorst and H. W. J. Blöte for very illuminating conversations concerning their work in Ref. 9, and P. Nozières for first interesting him in the model of Eq. (2). W.F.S. also wishes to thank the Aspen Center for Physics for its hospitality and stimulating environment, where this work was written for publication. This work was supported in part by National Science Foundation Grant No. DMR-84-04961.

APPENDIX

The model of Eq. (2) is readily analyzed via the momentum-space renormalization technique already developed by several authors.¹⁰⁻¹³ Under the length rescaling $r \rightarrow r'(1+\epsilon)$ one finds

$$\frac{d\sigma}{d\epsilon} = \left[V_1^2 + \frac{V_2^2}{16} \right] \frac{2\pi^4 c_3}{b^4 \sigma}, \quad (\text{A1})$$

$$\frac{dV_1}{d\epsilon} = \left[2 - \frac{\pi k_B T}{\sigma b^2} - \frac{c_1 V_2^2 \pi^2}{4V_1 \sigma b^2} \right] V_1, \quad (\text{A2})$$

$$\frac{dV_2}{d\epsilon} = \left[2 - \frac{\pi k_B T}{4\sigma b^2} - \frac{c_1 V_1 \pi^2}{\sigma b^2} \right] V_2, \quad (\text{A3})$$

where^{13b}

$$c_1 = \int_0^1 x J_0(x) dx \approx 0.44$$

and

$$c_3 = \int_0^1 x^3 J_0(x) dx \approx 0.21$$

are constants.²⁶ Note that Eq. (A3) is the form taken by Eq. (8) off the fixed line of the $V_2=0$ problem.

It is convenient to make the change of variables

$$\begin{aligned} X &= \frac{\sigma - A}{A}, \quad A \equiv \frac{\pi k_B T}{8b^2}, \\ W &= \frac{\pi^2 \sqrt{c_3} V_1}{2Ab^2}, \\ Y &= \frac{\pi^2 \sqrt{c_3} V_2}{4Ab^2}, \end{aligned} \quad (\text{A4})$$

in Eqs. (A1)–(A3) to obtain

$$\frac{dX}{d\epsilon} = \frac{8W^2 + 2Y^2}{X+1}, \quad (\text{A5})$$

$$\frac{dW}{d\epsilon} = \frac{2W}{X+1}(X-3) - \frac{2BY^2}{X+1}, \quad (\text{A6})$$

$$\frac{dY}{d\epsilon} = \frac{2Y}{X+1}(X+BW), \quad (\text{A7})$$

where²⁶ $B = c_1/\sqrt{c_3} \approx 0.96$. These three renormalization-group (RG) equations clearly exhibit a fixed line on the X axis, and no other fixed points. Considering both Y and $W \ll 1$ we further note that the fixed line is attractive for $X < 0$ (high temperature). Since trajectories in this region terminate at potential strengths of zero, the surface is rough. Also, for $X > 3$ (low temperature) both potential strengths grow with rescaling and the surface is smooth.

We now examine in greater detail the region $0 < X < 3$ which corresponds to $T_{R_1} < T < T_{R_2}$. In this range, Y always grows with rescaling, and the surface is thus always pinned (see Fig. 3). We therefore associate T_{R_2} with the true roughening temperature of the two-potential system. Analogous to the one-potential case, T_{R_2} is found by considering $V_1, V_2 \rightarrow 0$, and $X \rightarrow \bar{X} = 0$, where \bar{X} is the limiting value of X as $\epsilon \rightarrow \infty$. When $\bar{X} = 0$ we have

$$k_B T_{R_2} = \frac{8}{\pi} b^2 \bar{\sigma}(T_{R_2}), \quad (\text{A8})$$

where $\bar{\sigma}(T_{R_2})$ is the macroscopic surface stiffness at the roughening temperature. This universal result is in exact agreement with the one-potential case, realizing that the periodicity of the two-potential case is $2b$, resulting in a factor of 4 in Eq. (A8) compared to the one-potential result.

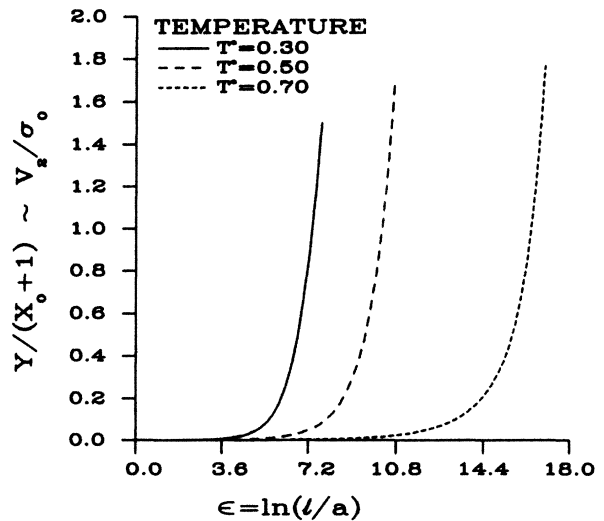


FIG. 3. Rescaling of the subharmonic potential V_2 in the temperature range $T_{R_1} < T < T_{R_2}$ with $V_2/\sigma_0 \sim Y_0/(X_0+1) = \frac{1}{3} \times 10^{-4}$, $V_1/\sigma_0 \sim W_0/(X_0+1) = \frac{1}{3} \times 10^{-1}$, and $T^* \equiv 1/(X_0+1) \sim T/\sigma_0$.

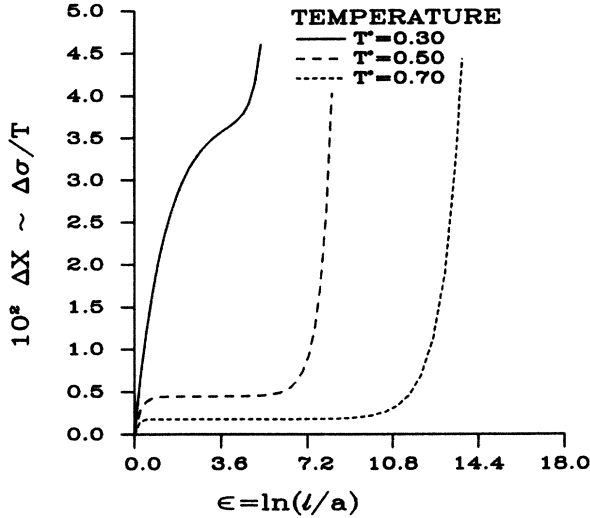


FIG. 4. Change in surface stiffness, $\Delta\sigma \equiv (\sigma - \sigma_0)$, with rescaling in the temperature range $T_{R_1} < T < T_{R_2}$ with $V_2/\sigma_0 \sim Y_0/(X_0+1) = \frac{1}{3} \times 10^{-4}$, $V_1/\sigma_0 \sim W_0/(X_0+1) = \frac{1}{3} \times 10^{-1}$, and $T^* \equiv 1/(X_0+1) \sim T/\sigma_0$.

When the initial value of Y (Y_0) is on the order of or greater than the initial value of W (W_0), Y grows with rescaling, and W becomes negative [remaining smaller in magnitude than Y until the length scale reaches the correlation length and the perturbation approximation in the derivation of Eqs. (A5)–(A7) breaks down].

The case of central interest here is $Y_0 \ll W_0 < 1$. Early in the rescaling, W approaches zero as ϵ increases as

$$W = \exp \left[\frac{2(X_0 - 3)\epsilon}{X_0 + 1} \right] \quad (\text{A9})$$

and X approaches a constant \bar{X} given by

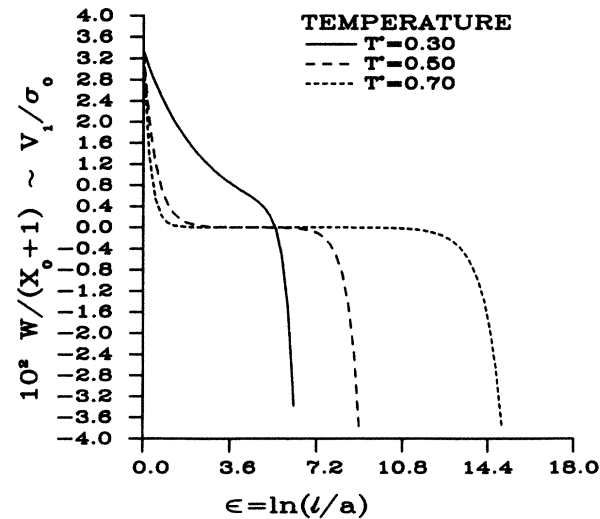


FIG. 5. Rescaling of V_1 in the temperature range $T_{R_1} < T < T_{R_2}$ with $V_2/\sigma_0 \sim Y_0/(X_0+1) = \frac{1}{3} \times 10^{-4}$, $V_1/\sigma_0 \sim W_0/(X_0+1) = \frac{1}{3} \times 10^{-1}$, and $T^* \equiv 1/(X_0+1) \sim T/\sigma_0$.

TABLE 1. Numerical check of $\ln \xi^{-1} \propto \ln Y_0$. R is the linear correlation coefficient.

Temperature	Least-squares fit Slope	R	Slope from Eq. (A15)
0.30	0.7106	1	0.7108
0.50	0.9978	1	0.9978
0.70	1.6619	1	1.6619

$$\bar{X} = 3 - [(X_0 - 3)^2 - 4W_0^2]^{1/2}, \quad (\text{A10})$$

provided Y remains small (see Figs. 3–5). This condition is satisfied for Y_0 sufficiently small, as will be made explicit below. \bar{X} is the terminal value of X on the trajectory of the one-potential case $Y_0 = 0$. While X stays at \bar{X} , Y grows as

$$Y = Y_0 \exp \left[\frac{2\bar{X}\epsilon}{\bar{X} + 1} \right]. \quad (\text{A11})$$

This is just the integral of Eq. (8), and the exponent $y_2 = 2\bar{X}/(\bar{X} + 1)$. Eventually, Y reaches W_0 and both X and W begin to change again.

The scenario of the preceding paragraph holds if Y_0 is sufficiently small. To determine how small, note that if W is driven to e^{-2} of its initial value,

$$\epsilon \gtrsim \frac{X_0 + 1}{3 - X_0}, \quad (\text{A12})$$

while if Y is to remain $< W_0$,

$$\epsilon \lesssim \frac{X_0 + 1}{2X_0} \ln \frac{W_0}{Y_0}, \quad (\text{A13})$$

where we have ignored the small difference (for small V_1) between X_0 and \bar{X} . Combination of the last two results gives

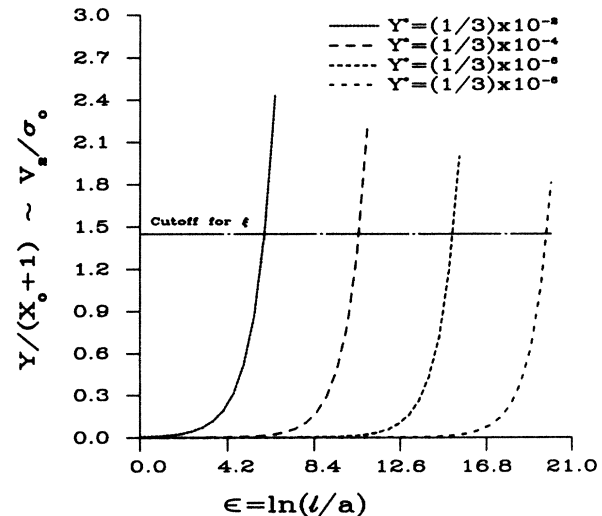


FIG. 6. Rescaling of V_2 for several initial values of $V_2/\sigma_0 \sim Y^* \equiv Y_0/(X_0+1)$ at $T^* \equiv 1/(X_0+1) = 0.5$, $V_1/\sigma_0 \sim W_0/(X_0+1) = \frac{1}{3} \times 10^{-1}$.

$$X_0 \lesssim \frac{3 \ln(W_0/Y_0)}{2 + \ln(W_0/Y_0)}, \quad (\text{A14})$$

which is satisfied for W_0/Y_0 sufficiently large, noting that $X_0 < 3$ if $T > T_{R_1}$.

Numerical integration of the RG equations (A5)–(A7) was performed for

$$W_0/(X_0+1) = \frac{1}{3} \times 10^{-1}$$

and

$$Y_0/(X_0+1) = \frac{1}{3} \times 10^{-4},$$

where $W_0/(X_0+1)$ and $Y_0/(X_0+1)$ are proportional to V_1/σ_0 and V_2/σ_0 , respectively (σ_0 denotes the initial value of σ). Figures 3–5 show the behavior of the potentials as a function of $\epsilon = \ln(l/a)$ for various temperatures [$1/(X_0+1) \propto T/\sigma_0$]. For temperatures consistent with condition (A14), indeed $W \rightarrow 0$ and $(X - X_0) \rightarrow (\bar{X} - X_0)$

before Y finally becomes significant.

The correlation length was determined as the value of l where $Y/(X_0+1) = 1.45$ (where $V_2/k_B T \sim 1$). Figure 6 of $Y/(X_0+1)$ as a function of ϵ shows that at a given temperature, $\ln \xi^{-1}$ increases linearly with $\ln[Y_0/(X_0+1)]$. This is consistent with the determination of ξ from Eq. (A11) [$Y \sim 1$ at $\epsilon = \ln(l/a) = \ln(\xi/a)$]

$$\frac{\xi}{b} = Y_0^{-[(1+\bar{X})/2\bar{X}]} \quad (\text{A15})$$

Furthermore, this relation is independent within an order of magnitude of the choice of the $Y/(X_0+1)$ used to determine ξ . For values of $Y_0/(X_0+1)$ from $\frac{1}{3} \times 10^{-2}$ to $\frac{1}{3} \times 10^{-10}$, subject to Eq. (A14), the results of a least-squares fit of $\ln \xi^{-1}$ versus $\ln Y_0$ for three temperatures [$T/\sigma_0 \propto 1/(X_0+1) = 0.3, 0.5, 0.7$] are summarized in Table I. The linear correlation coefficient, R , shows that the relation is indeed linear, and the slopes have excellent agreement with Eq. (A15).

¹P. E. Wolf, F. Gallet, S. Balibar, E. Rolley, and P. Nozières, *J. Phys. (Paris)* **46**, 1987 (1985).

²F. Gallet, S. Balibar, and E. Rolley, *J. Phys. (Paris)* **48**, 369 (1987).

³F. Gallet, P. Nozières, S. Balibar, and E. Rolley, *Europhys. Lett.* **2**, 701 (1986).

⁴A. V. Babkin, D. B. Kopeliovich, and A. Ya. Parshin, *Zh. Eksp. Teor. Fiz.* **89**, 2288 (1985) [*Sov. Phys.—JETP* **62**, 1322 (1985)].

⁵A recent review is C. Rottman and M. Wortis, *Phys. Rep.* **103**, 59 (1984).

⁶C. Jayaprakash, W. F. Saam, and S. Teitel, *Phys. Rev. Lett.* **50**, 2017 (1983).

⁷C. Jayaprakash and W. F. Saam, *Phys. Rev. B* **30**, 3916 (1984).

⁸C. Jayaprakash, C. Rottman, and W. F. Saam, *Phys. Rev. B* **30**, 6549 (1984).

⁹B. Nienhuis, H. J. Hilhorst, and H. W. Blöte, *J. Phys. A* **17**, 3559 (1984).

¹⁰P. Nozières and F. Gallet, *J. Phys. (Paris)* **48**, 353 (1987).

¹¹H. J. F. Knops and L. W. J. den Ouden, *Physica* **103A**, 597 (1980).

¹²H. J. F. Knops, in *Fundamental Problems in Statistical Mechanics V*, edited by E. G. D. Cohen (North-Holland, Amsterdam, 1980), p. 7.

¹³(a) T. Ohta and K. Kawasaki, *Prog. Theor. Phys.* **60**, 365 (1978); (b) T. Ohta, *ibid.* **60**, 968 (1978).

¹⁴B. Nienhuis, H. J. Hilhorst, and H. W. Blöte (see Ref. 9) have suggested NaCl as a possible example. However, {111} facets

do not belong to its equilibrium form (see Ref. 15).

¹⁵An-Chang Shi and M. Wortis, *Phys. Rev. B* (to be published).

¹⁶B. K. Vainstein, V. M. Fridkin, and V. L. Indenbom, *Modern Crystallography II* (Springer-Verlag, New York, 1982), p. 162.

¹⁷J. P. Suchet, *Crystal Chemistry and Semiconduction in Transition Metal Binary Compounds* (Academic, London, 1971), pp. 27–29.

¹⁸C. Palache, H. Berman, and C. Frondel, *The System of Mineralogy of James Dwight Dana and Edward Salisbury Dana, 7th ed.* (Wiley, New York, 1944), Vol. 1, pp. 200–207.

¹⁹Gunther A. Wolff, in *Intermetallic Compounds*, edited by J. H. Westbrook (Wiley, New York, 1967), pp. 85–99; G. A. Wolff, M. Weinstein, and B. N. Das, *J. Crystal. Growth* **13/14**, 186 (1979).

²⁰See, e.g., the review article by E. H. Lieb and F. Y. Wu, in *Phase Transitions and Critical Phenomena*, edited by C. Domb and M. S. Green (Academic, London, 1972), Vol. 1.

²¹D. S. Fisher and J. D. Weeks, *Phys. Rev. Lett.* **59**, 1077 (1983).

²²See, e.g., the review by B. Nienhuis, *J. Stat. Phys.* **34**, 731 (1984), as well as Ref. 12.

²³H. van Beijeren, *Phys. Rev. Lett.* **38**, 993 (1977).

²⁴R. J. Baxter, *Phys. Rev. B* **1**, 2199 (1970).

²⁵See, e.g., Ref. 7 where this point is discussed in detail in a related context.

²⁶As shown in Refs. 10 and 11, the “constants” c_1 , c_3 , and, therefore, B should really have some smooth temperature dependence. This dependence is unimportant for any conclusions of the paper, and we ignore it for simplicity.